

Three-dimensional hybrid photonic crystals merged with localized plasmon resonances

Jiafang Li^{1,2}, MD Muntasir Hossain¹, Baohua Jia¹, Dario Buso¹ and Min Gu^{1*}

¹Centre for Micro-Photonics and CUDOS, Faculty of Engineering and Industrial Sciences, Swinburne University of Technology, Hawthorn, Victoria 3122, Australia

²Laboratory of Optical Physics, Institute of Physics, Chinese Academy of Sciences, Beijing 100190, China
*mgu@swin.edu.au

Abstract: Localized plasmon resonances are proposed in a new concept of 3D photonic crystals stacked by hybrid rods made of dielectric-cores and metallic-nanoshells. The resonant plasmon coupling of inner and outer surfaces of the metallic-nanoshells forms the localized plasmon resonances which can be flexibly tuned by mediating the dielectric cores. At the resonance wavelengths, the strong electromagnetic wave-plasmon interaction leads to the enhancement in the structural absorption by more than 20 times. The tunability of the enhanced absorption is demonstrated in experiments.

©2010 Optical Society of America

OCIS codes: (230.5298) Photonic crystals; (220.4000) Microstructure fabrication; (250.5403) Plasmonics; (310.3915) Metallic coatings.

References and links

1. J. G. Fleming, S.-Y. Lin, I. El-Kady, R. Biswas, and K. M. Ho, "All-metallic three-dimensional photonic crystals with a large infrared bandgap," *Nature* **417**(6884), 52–55 (2002).
2. I. El-Kady, M. M. Sigalas, R. Biswas, K. M. Ho, and C. M. Soukoulis, "Metallic photonic crystals at optical wavelengths," *Phys. Rev. B* **62**(23), 15299–15302 (2000).
3. S. Y. Lin, J. G. Fleming, Z. Y. Li, I. El-Kady, R. Biswas, and K. M. Ho, "Origin of absorption enhancement in a tungsten, three-dimensional photonic crystal," *J. Opt. Soc. Am. B* **20**(7), 1538–1541 (2003).
4. S. Y. Lin, J. G. Fleming, E. Chow, J. Bur, K. K. Choi, and A. Goldberg, "Enhancement and suppression of thermal emission by a three-dimensional photonic crystal," *Phys. Rev. B* **62**(4), R2243–R2246 (2000).
5. S. Y. Lin, S. Moreno, and G. R. Fleming, "Three-dimensional photonic-crystal emitter for thermal photovoltaic power generation," *Appl. Phys. Lett.* **83**(2), 380–382 (2003).
6. C.-Y. Kuo, and S.-Y. Lu, "Opaline metallic photonic crystals possessing complete photonic band gaps in optical regime," *Appl. Phys. Lett.* **92**(12), 121919 (2008).
7. M. S. Rill, C. Plet, M. Thiel, I. Staude, G. von Freymann, S. Linden, and M. Wegener, "Photonic metamaterials by direct laser writing and silver chemical vapour deposition," *Nat. Mater.* **7**(7), 543–546 (2008).
8. S. Y. Lin, D.-X. Ye, T.-M. Lu, J. Bur, Y. S. Kim, and K. M. Ho, "Achieving a photonic band edge near visible wavelengths by metallic coatings," *J. Appl. Phys.* **99**(8), 083104 (2006).
9. V. Mizeikis, S. Juodkazis, R. Tarožaitė, J. Juodkazytė, K. Juodkazis, and H. Misawa, "Fabrication and properties of metallo-dielectric photonic crystal structures for infrared spectral region," *Opt. Express* **15**(13), 8454–8464 (2007).
10. A. Tal, Y. S. Chen, H. E. Williams, R. C. Rumpf, and S. M. Kuebler, "Fabrication and characterization of three-dimensional copper metallodielectric photonic crystals," *Opt. Express* **15**(26), 18283–18293 (2007).
11. C. Luo, S. Johnson, J. Joannopoulos, and J. Pendry, "Negative refraction without negative index in metallic photonic crystals," *Opt. Express* **11**(7), 746–754 (2003).
12. A. Mahmoudi, A. Semnani, R. Alizadeh, and R. Adeli, "Negative refraction of a three-dimensional metallic photonic crystal," *Eur. Phys. J. Appl. Phys.* **39**(1), 27–32 (2007).
13. J. Lourtioz, "Les cristaux photoniques métalliques," *C. R. Phys.* **3**(1), 79–88 (2002).
14. W. L. Barnes, A. Dereux, and T. W. Ebbesen, "Surface plasmon subwavelength optics," *Nature* **424**(6950), 824–830 (2003).
15. E. Ozbay, "Plasmonics: merging photonics and electronics at nanoscale dimensions," *Science* **311**(5758), 189–193 (2006).
16. P. Zijlstra, J. W. Chon, and M. Gu, "Five-dimensional optical recording mediated by surface plasmons in gold nanorods," *Nature* **459**(7245), 410–413 (2009).
17. Z. Y. Li, I. El-Kady, K. M. Ho, S. Y. Lin, and J. G. Fleming, "Photonic band gap effect in layer-by-layer metallic photonic crystals," *J. Appl. Phys.* **93**(1), 38–42 (2003).
18. F. Hallermann, C. Rockstuhl, S. Fahr, G. Seifert, S. Wackerow, H. Graener, G. V. Plessen, and F. Lederer, "On the use of localized plasmon polaritons in solar cells," *Phys. Status Solidi A* **205**(12), 2844–2861 (2008).

19. E. Prodan, C. Radloff, N. J. Halas, and P. Nordlander, "A hybridization model for the plasmon response of complex nanostructures," *Science* **302**(5644), 419–422 (2003).
 20. T. V. Teperik, F. J. García De Abajo, A. G. Borisov, M. Abdelsalam, P. N. Bartlett, Y. Sugawara, and J. J. Baumberg, "Omnidirectional absorption in nanostructured metal surfaces," *Nat. Photonics* **2**(5), 299–301 (2008).
 21. M. Straub, and M. Gu, "Near-infrared photonic crystals with higher-order bandgaps generated by two-photon photopolymerization," *Opt. Lett.* **27**(20), 1824–1826 (2002).
 22. M. Deubel, G. von Freymann, M. Wegener, S. Pereira, K. Busch, and C. M. Soukoulis, "Direct laser writing of three-dimensional photonic-crystal templates for telecommunications," *Nat. Mater.* **3**(7), 444–447 (2004).
 23. S. Wong, M. Deubel, F. Pérez-Willard, S. John, G. A. Ozin, M. Wegener, and G. von Freymann, "Direct laser writing of three-dimensional photonic crystals with a complete photonic band gap in chalcogenide glasses," *Adv. Mater.* **18**(3), 265–269 (2006).
 24. R. F. Service, "Solar energy. Can the upstarts top silicon?" *Science* **319**(5864), 718–720 (2008).
 25. J. R. Reitz, F. J. Milford, and R. W. Christy, *Foundations of Electromagnetic Theory*, 4th ed. (Addison-Wesley, Reading, 1993).
 26. P. Nagpal, S. E. Han, A. Stein, and D. J. Norris, "Efficient low-temperature thermophotovoltaic emitters from metallic photonic crystals," *Nano Lett.* **8**(10), 3238–3243 (2008).
 27. Y.-S. Chen, A. Tal, D. B. Torrance, and S. M. Kuebler, "Fabrication and characterization of three-dimensional silver-coated polymeric microstructures," *Adv. Funct. Mater.* **16**(13), 1739–1744 (2006).
 28. J. Li, B. Jia, G. Zhou, and M. Gu, "Fabrication of three-dimensional woodpile photonic crystals in a PbSe quantum dot composite material," *Opt. Express* **14**(22), 10740–10745 (2006).
 29. S. Noda, M. Fujita, and T. Asano, "Spontaneous-emission control by photonic crystals and nanocavities," *Nat. Photonics* **1**(8), 449–458 (2007).
 30. M. J. Ventura, and M. Gu, "Engineering spontaneous emission in a quantum dot-doped polymer nanocomposite with three-dimensional photonic crystals," *Adv. Mater.* **20**(7), 1329–1332 (2008).
-

1. Introduction

Three-dimensional (3D) metallic photonic crystals (MPCs), either all-metallic [1–6] or partial-metallic (sometimes called "metallodielectric") [7–10] MPCs, are artificial structures formed by arranging metallic elements in three dimensions. Due to the strong discontinuities of the dielectric function at the metal/air or metal/dielectrics interfaces, 3D MPCs offer intriguing electromagnetic (EM) properties and important applications such as enhanced metal absorption [3], modified blackbody radiation [4, 5], ultra-wide complete photonic band gaps [1, 2, 6], negative refraction [11, 12] and microwave circuits [13]. On the other hand, plasmonics [14, 15], one of the most important characters in metallic systems, provides a promising new way to control the photon-matter interaction at a nanometer scale and has wide applications in high-density optical data storage [16], near-field optics and surface-enhanced Raman spectroscopy [14]. The major problem in all the current 3D MPCs is that the metallic rods or metallic layers in those MPCs have been employed with thickness far thicker than the skin depth of the metals, which excluded the penetration of EM waves into the rods or layers [1, 10, 17] and resulted in the lack of the plasmonic effects, such as localized plasmon resonances (LPRs) [18].

Here we propose and study for the first time a new type of 3D hybrid photonic crystal (HPC) that possesses not only strong photonic band gaps (PBGs) but also significant LPRs due to the existence of the metallic nanoshells coated on the dielectric rods. The proposed 3D HPCs merged with LPRs are conceptually different from the spherical nanoshells [19] and nanovoids [20] in the sense that in the latter cases there are no PBG effects. Moreover, our 3D HPCs are straightforward for fabrications using the well-established two-photon polymerization (2PP) technique [7, 21–23] and thus can lead to breakthrough functionalities of both 3D photonic crystals and plasmonics [24].

2. Modelling

2.1 Two-dimensional hybrid rods

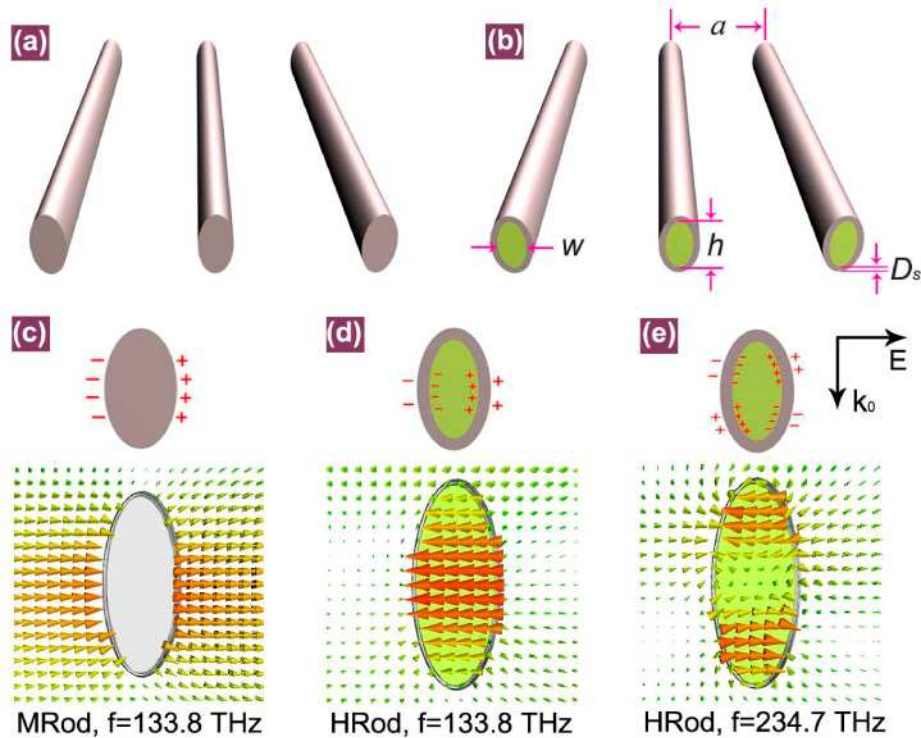


Fig. 1. (a, b) Schematic of parallel MRods (a) and HRods (b). The HRod consists of a dielectric rod (with width w , height h , rod spacing a , refractive index n) and a silver nanoshell (with thickness D_s). (c, d, e) Schematic of the charge density distributions (top panels) and snapshots of the calculated E-field (linear scale, bottom panels) in the cross-section for an MRod (c) and an HRod (d, e) at the noted frequency. The distributions of the E-field correspond well to the charge distributions. HRod parameters: $w=240\text{ nm}$, $h=2.5w$ (for all calculations in this article), $a=1\text{ }\mu\text{m}$, $D_s=10\text{ nm}$ and $n=1.56$. MRods are calculated based on the HRod parameters by replacing dielectrics with silver. All simulation results in this paper are carried with the software package CST Microwave Studio. For simplicity, we use silver with permittivity described by the Drude model with plasma frequency $\omega_{pl}=1.37\times 10^{16}\text{ s}^{-1}$ and collision frequency $\omega_{col}=8.5\times 10^{13}\text{ s}^{-1}$ [7].

The principle of hybrid rods (HRods) that are used to form the 3D HPCs are shown in Fig. 1. Figure 1(a), 1(b) shows parallel elliptical metallic rods (MRods) and HRods, respectively. HRods, as illustrated in Fig. 1(b), can be formed by coating ultra-thin silver nanoshells ($D_s \sim 10\text{-}20\text{ nm}$) on elliptical dielectric rods and are the basic elements to form 3D HPCs. It is well known that when p-polarized light interacts with a metal/dielectric interface, charge density oscillations are introduced as plasmons [14, 15]. In the case of MRods [Fig. 1(a)], the resultant plasmons are difficult to form resonances due to the lack of confinement [Fig. 1(c)]. However, for the HRods, plasmons can be coupled from the outer surfaces to the inner surfaces of the nanoshells due to the small thickness which is comparable with the skin depth ($\sim 22\text{ nm}$ at wavelength $1.5\text{ }\mu\text{m}$ by calculation [25]). Due to the close loop of the rod cross-section, the surface charges which are localized on the inner and outer surfaces of the nanoshells form ring-cavity-like plasmon resonances [Fig. 1(d)]. As a result, the localized electric-field (E-field) can be formed inside the HRods.

Figure 1(c), 1(d) (bottom panels) shows the simulated E-field distributions around an MRod and an HRod under the same light excitation, respectively. The E-field maps (bottom

panels) confirm that the E-field cannot exist within an MRod as expected but can exist inside an HRod at certain resonance frequency. It is this internal E-field that facilitates the charge distribution on the inner and outer surfaces of the nanoshells as illustrated in Fig. 1(c), 1(d) (top panels), which verifies the excitation of LPRs in HRods. It should be mentioned that higher-order LPRs at higher frequencies also exist, as pictured in Fig. 1(e). At the LPR frequencies/wavelengths, due to the back and forth coupling between EM waves and plasmons as well as the coupling between plasmons on the inner and outer surfaces of the nanoshells, the EM wave-plasmon interaction in HRods is significantly enhanced. As a result, the absorption of HRods can be greatly enhanced at the LPRs.

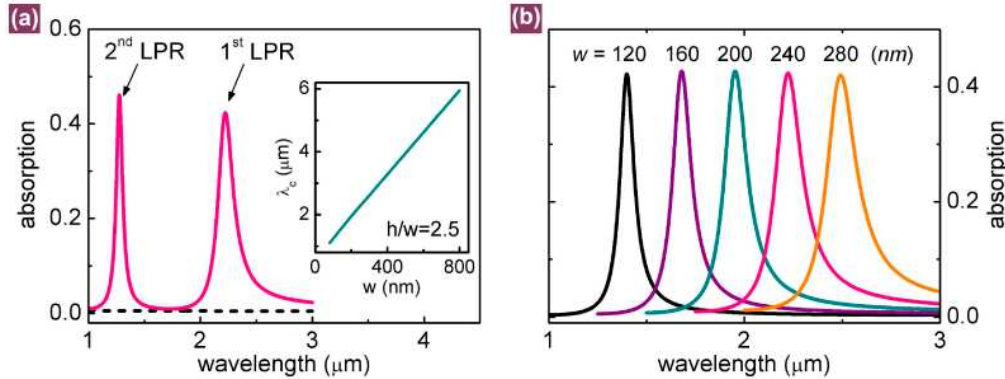


Fig. 2. (a) Calculated absorption spectra of the HRods (solid line) and MRods (dashed line) with the same parameters in Fig. 1c-e. Inset: Center wavelength (λ_c) of the 1st order LPR versus the dielectric rod width (w) for $a=1 \mu\text{m}$, $w=240 \text{ nm}$, $D_s=10 \text{ nm}$, $n=1.56$. (b) Calculated LPR absorption spectra of HRods with different w as noted. For the different values of w , the ratio h/w is kept constant at 2.5. Variations in peak values are less than 1.2%. Other calculation parameters are the same as those in (a). Here the absorption is simply defined as $1-R-T$, where R and T are the calculated reflection and transmission intensities. The calculated reflection and transmission intensity spectra are determined from the reflection and transmission coefficients, respectively, which are obtained with the CST software package.

The corresponding absorption spectra of the HRods in Fig. 1(c), 1(d) are displayed in Fig. 2(a). It indeed shows that two LPR-enhanced absorption channels emerging at the corresponding LPR wavelengths, where the enhancement factors are ~ 82 and ~ 83 at the 1st and 2nd order LPR wavelengths, respectively, compared with the absorption of the MRods. The higher-frequency or higher-order LPRs are very useful to create multiple absorption channels and advantageous to extend the operating wavelengths to the visible wavelength range. However, to simplify the analysis, we consider only the 1st order LPR in the following discussion.

It is important to point out that the position of the LPR is extremely sensitive to the rod parameters. As shown in the inset of Fig. 2(a), the LPR wavelength (λ_c) can be linearly tuned from 1.1 to 6.0 μm by increasing the rod width w from 80 to 800 nm, while the strength of the LPR absorption remains constant [Fig. 2(b)]. Similarly, increasing the refractive index of the dielectric cores or decreasing the silver shell thickness (D_s) will also result in the increase of λ_c (not shown). However, our simulations show that the LPR becomes negligible for $D_s > 60 \text{ nm}$, which is mainly caused by the weak plasmon coupling between the inner and outer surfaces as D_s is 2-3 times of corresponding skin depth. This is the main reason why the LPRs have never been discovered in all the current 3D MPCs [1, 2, 10, 17].

2.2 Three-dimensional hybrid photonic crystals

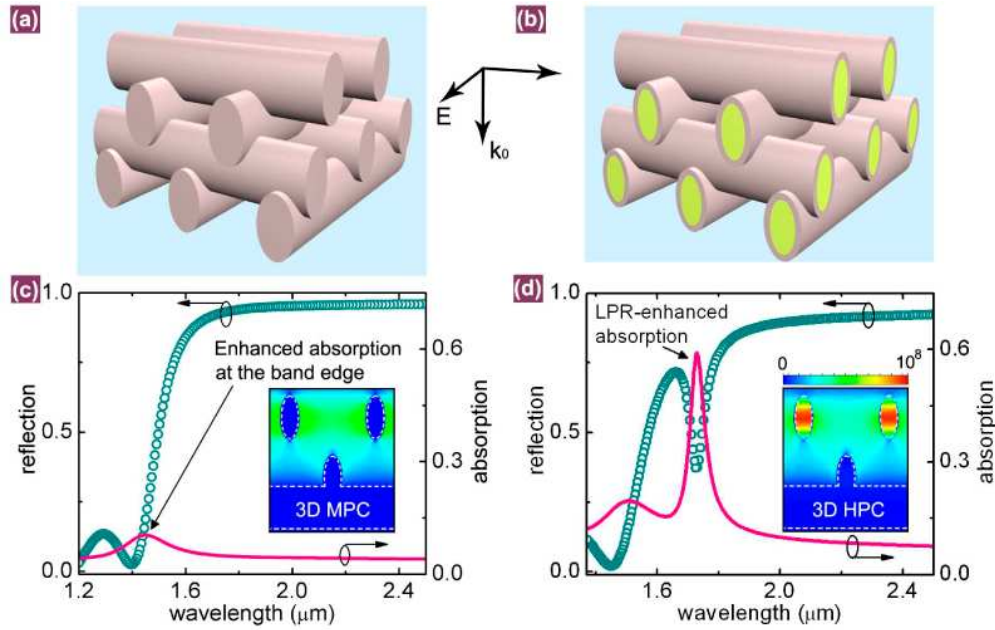


Fig. 3. (a, b) Schematic of a 3D MPC (a) and a 3D HPC (b) of four layers with an in-plane rod spacing of a and a four-layer height of c ($c=1.414a$). In following simulations, the incident light is linearly polarized perpendicular to the first-layer rods. (c, d) Calculated reflection (circle) and absorption (solid line) spectra of a 3D MPC (c) and a 3D HPC (d). Inset: Calculated spatial distribution of the amplitude of the E-field inside a 3D MPC and a 3D HPC at wavelength $1.73 \mu\text{m}$ (the cross-sections are perpendicular to the first-layer rods and the outlines of the rods are denoted by the dashed lines; the field amplitude is normalized to the color bar in the inset of Fig. d). Simulation parameters of the HPC: $a=1 \mu\text{m}$, $w=200 \text{ nm}$, $D_s=20 \text{ nm}$, $n=1.56$; the MPC is based on the corresponding HPC by replacing dielectrics with silver.

Figure 3(a), 3(b) illustrates the schematic of 3D woodpile MPC and HPC structures of a face-centered-cubic geometry. Due to the existence of LPRs in HRods, the E-field inside the 3D HPC is strongly localized at the LPR wavelength [see the inset of Fig. 3(c), 3(d)], while at other wavelengths the HPC behaves similarly as the MPC (not shown). As a result, the 3D HPC shows significant spectral differences compared with the 3D MPC. As shown in Fig. 3(c), the 3D MPC has a high reflection region above wavelength $1.6 \mu\text{m}$ and a band edge region at wavelength $1.45 \mu\text{m}$, where an enhanced absorption channel is created due to the slow light effect [3]. Impressively, in addition to the enhanced absorption peak at the band edge, there exists an LPR-enhanced absorption peak in the 3D HPC. This peak absorption (A_{max}) reaches 0.59 at wavelength $1.73 \mu\text{m}$ [Fig. 3(d)], which is ~ 12 times of the absorption of the MPC and ~ 23 times of the absorption of a 20-nm silver film, respectively, at wavelength $1.73 \mu\text{m}$. Meanwhile, the density of this absorption channel, defined as A_{max}/W_{FWHM} (W_{FWHM} is the full width at half maximum of the absorption channel), is enhanced by ~ 29 times compared with the absorption channel at the band edge of the MPC.

One unique feature of our 3D HPCs is that the positions of the LPR and the PBG of the structure can be “independently” tuned by the dielectric refractive index of the rods and the rod spacing, respectively. As shown in Fig. 4(a), the LPR wavelength (λ_c) is tuned from the left side to the right side of the band edge by increasing the refractive index from 1.0 to 1.56, resulting in the red-shift of λ_c by $\sim 730 \text{ nm}$. It is noticed that the absorption peak at the band edge does not change with the dielectric refractive index because it results from the PBG effects [3] that are only dependent on the periodic metallic part. On the other hand, the strength of the LPRs is enhanced by the PBGs of the 3D HPCs. To demonstrate the PBG

effect in this aspect, we directly compare the enhancement in A_{max} when the simulated structure is changed from a 2D HRod array to a 3D HPC. Figure 4(b) illustrates this absorption enhancement, i.e. $A_{max-HPC}/A_{max-HRod}$, as a plot of λ_c which is linearly tuned by changing the refractive index. This wavelength-dependent change in the absorption enhancement unambiguously reflects the PBG effects on the strength of the LPR-enhanced absorption. Particularly, the absorption enhancement reaches a maximum at the low-energy band edge of the 3D HPC while it approaches a minimum at the high-energy band edge [Fig. 4(b)]. The effect of the PBG is further manifested by tuning the rod spacing a . As shown in Fig. 4(b), when the band edge positions (as noted by the arrows) blue-shift with decreased a , the absorption enhancement curve shifts correspondingly towards shorter wavelengths. Apart from the refractive index of the dielectric rods, the thickness of the silver nanoshells and the filling ratio (w/a) of the dielectric rods also play very important roles in engineering the LPR-enhanced absorption of HPCs (not shown). For example, by decreasing D_s to 8 nm ($a=1 \mu\text{m}$, $w=160 \text{ nm}$, $n=1.4$), the LPR-enhanced absorption can reach as high as ~ 0.93 .

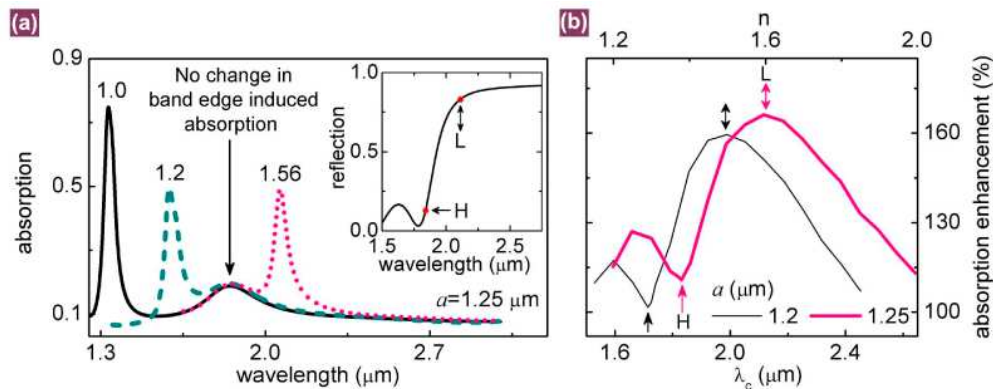


Fig. 4. (a) Calculated absorption spectra of 3D HPCs for different refractive indices (n) of the embedded dielectrics at 1.0, 1.2 and 1.56. Inset: Typical reflection spectrum of a HPC. The band edge region is distinguished as a high-energy edge (H point, corresponding to the band edge in Fig. 3(c)) and a low-energy edge (L point). (b) Absorption enhancement [$A_{max-HPC}/A_{max-HRod}$] between 3D HPCs and 2D HRods as a function of the LPR wavelength (λ_c) under different rod spacing a . $A_{max-HPC}$ and $A_{max-HRod}$ are the LPR-enhanced absorption of 3D HPCs and 2D HRods, respectively. The value of λ_c (bottom axis) and the corresponding enhancement factor are obtained when n (top axis) is tuned, which follows a linear relation by $\lambda_c=0.0134+1.317n$. The single-headed and double-headed arrows indicate the wavelength positions of the high-energy (H) and low-energy (L) band edges of the 3D HPC, respectively. The wavelength- and lattice-dependent absorption enhancement clearly illustrates the PBG effects on the LPR-enhanced absorption. Calculation parameters: $w=250 \text{ nm}$, $D_s=20 \text{ nm}$.

3. Experiments

The proposed LPR-merged 3D HPCs can be fabricated by applying the versatile metallization methods [7–10, 26,27] on 3D dielectric PC (DPC) templates generated with the sophisticated direct laser writing techniques [7, 21–23]. We demonstrate this feasibility by firstly fabricating a 3D DPC with the 2PP technique [21] and subsequently coating the DPC with an ultra-thin silver layer through an electroless silver deposition process [27]. As shown in Fig. 5(a), a silver layer (with averaged effective thickness of $\sim 15 \text{ nm}$) has been clearly deposited on the surfaces of a fabricated 3D polymeric woodpile PC. As a result, the reflection spectrum of the 3D HPC in Fig. 5(b) shows a high reflection region at longer wavelengths which represents the band gap characteristic of 3D MPCs and a “dip” within the high reflection region which indicates the existence of the LPR at wavelength $\sim 1.7 \mu\text{m}$. Moreover, the absorption peak at this wavelength is enhanced by approximately 7.3 times compared with that of a silver layer. This feature is consistent with the theoretical simulations [Fig. 5(c)] in terms of the position and depth of the “dip”. The deviation of the measured

reflection and absorption spectra from the calculations is caused by the averaging effect in measurements [28], the roughness of the silver layers, and the scattering losses. In addition, the tunability of the LPR is further illustrated in Fig. 5(d), where the LPR wavelength is monotonically tuned by ~ 240 nm when simply increasing the dielectric rod width by ~ 82 nm while keeping the lattice unchanged. It can be seen that for the three HPCs, HPC(II) shows a more pronounced absorption peak than the others. This is because the LPR of the HPC(II) is located at the low-energy band edge of the HPC [as shown in Fig. 5(b)], where the maximal absorption enhancement occurs [as illustrated in Fig. 4(b)]. When the width of the dielectric rod is changed, the position of the LPR is tuned away from the corresponding low-energy band edges, which results in the drop of the absorption enhancement [Fig. 4(b)] and thus the decrease in the strength of the absorption peak. It should be mentioned that here the bulk properties of the metal have been expressed by the Drude model which characterizes the free electrons in metal as damped harmonic oscillators. The damping causes the oscillating electrons to dissipate energy over their mean decay time. For the localized plasmon resonances in our cases the energy dissipation may become severe by the damping effect which could effectively result in nonradiative decay (Ohmic loss) in the form of heating. This may be beneficial to the studies including modified blackbody radiation [4] and efficient thermophotovoltaic emitters [5, 26] and can be measured by strict photoacoustic spectroscopy [1].

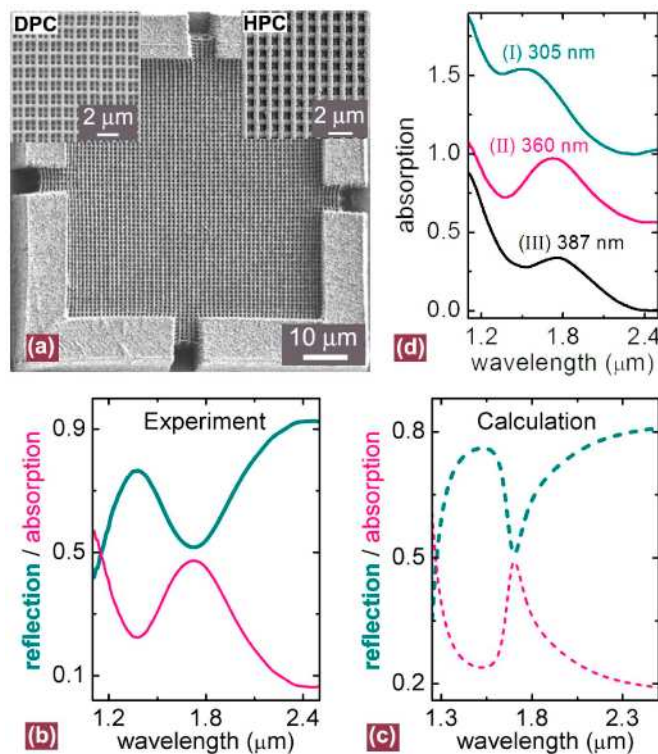


Fig. 5. (a) SEM image of a 3D polymeric woodpile DPC after the electroless silver deposition process [24]. Silver particles were nucleated on the surfaces of the DPC to form a 3D silver HPC. Inset: close view of the DPC and the HPC. (b, c) Measured and calculated reflection and absorption spectra of the 3D silver HPC in (a). Simulation parameters are $a=0.9 \mu\text{m}$, $w=360 \text{ nm}$, $h=510 \text{ nm}$, $D_s=15 \text{ nm}$ (in average), $n=1.47$, $\omega_{pl}=1.37 \times 10^{16} \text{ s}^{-1}$, and $\omega_{col}=1.7 \times 10^{14} \text{ s}^{-1}$, which fit best with our experimental conditions. (d) Experimental absorption spectra of 3D HPCs with different dielectric rod width as noted. The value of λ_c is tuned from $1.51 \mu\text{m}$ to $1.75 \mu\text{m}$ when the rod width increases from 305 nm to 387 nm . The spectra are vertically shifted for clear display.

4. Conclusions

In summary, we have both theoretically and experimentally demonstrated the concept of 3D HPCs. The resonant plasmon coupling of inner and outer surfaces of the metallic-nanoshells in 3D HPCs forms the LPRs which strongly interact with external field. Consequently, the structural absorption of the 3D HPCs can be enhanced by more than 20 times and can be widely tuned in spectra by mediating the dielectrics. The LPR-merged 3D HPCs can be immediately applied to a wide range of broadband tunable nanophotonic devices including surface enhanced Raman sensors [14, 15], 3D metamaterials [7] and energy harvesting systems [18, 24]. A straightforward study will be on the high-efficiency low-temperature thermophotovoltaics [26]. In addition, the strongly localized E-field inside the rods of HPCs provides a unique environment to explore optical nonlinearity and emission control [29] if the dielectric rods are functionalized [28, 30].

Acknowledgements

This work was produced with the assistance of the Australian Research Council (ARC) under the Centres of Excellence program. CUDOS (the Centre for Ultrahigh-bandwidth Devices for Optical Systems) is an ARC Centre of Excellence. Baohua Jia acknowledges the ARC for the support through the APD grant DP0987006. Dario Buso acknowledges the ARC for the support through the APD grant DP0988106.